Biomass-Derived High-Performance Tungsten-Based Electrocatalysts on Graphene for Hydrogen Evolution

Fanke Meng,[a] Enyuan Hu,[a] Lihua Zhang,[b] Kotaro Sasaki,[a,*]

James T. Muckerman,[a] and Etsuko Fujita[a,*]

[a] Chemistry Department, Brookhaven National Laboratory, Upton, New York, 11973, USA.

[b] Center for Functional Nanomaterials, Brookhaven National Laboratory, Upton, New York 11973, USA

Abstract

We report a new class of highly active and stable tungsten-based catalysts to replace noble metal materials for the hydrogen evolution reaction (HER) in an acidic electrolyte. The catalyst is produced by heating an earth-abundant and low-cost mixture of ammonium tungstate, soybean powder and graphene nanoplatelets (WSoyGnP). The catalyst compound consists of tungsten carbide (W_2C and WC) and tungsten nitride (WN) nanoparticles decorated onto graphene nanoplatelets. The catalyst demonstrates an overpotential (η_{10}, the potential at a current density of 10 mA cm^{-2}) of 0.105 V, which is the smallest among tungsten-based HER catalysts in acidic media. The coupling with graphene significantly reduces the charge transfer resistance and increases the active surface area of the product, which are favorable for enhancing the HER activity. Therefore, the approach of employing biomass and other less expensive materials as precursors for the production of catalysts with high HER activity provides a new path for the design and development of efficient catalysts for the hydrogen production industry.

1. Introduction

In comparison with fossil fuels, hydrogen is a green source of energy that does not generate carbon dioxide during direct combustion or in hydrogen fuel cells that could play an important role in meeting the growing energy needs of the world.[1–4] One attractive approach to generating hydrogen fuel is via the electrocatalytic hydrogen evolution reaction (HER) in splitting water.[4–8] In this scenario, developing efficient and durable electrocatalysts is extremely critical. Until now, Pt-group metals (Pt, Ir, Ru, Rh, Pd) have been the most efficient catalysts for

the HER for the reason that, as a typical example, Pt exhibits an optimal hydrogen binding energy to balance the hydrogen adsorption and release on the catalyst surface.[9–11] However, its precious nature and scarcity hinder scale-up production and market penetration of the noble metals to satisfy the goal of competitive hydrogen production ($2.00-3.00 kg^{-1}) of the U.S. Department of Energy.[12] For this reason, development of noble-metal-free materials to substitute for Pt-group catalysts to lower cost without a significant loss in catalytic activity is strongly motivated. Recently, a family of tungsten-based materials (WS_2, WSe_2, WP, WC, W_xC, etc.)[13–24] was extensively investigated as effective electrocatalysts for the HER because of favorable structural and electronic properties.[25,26] For example, as one of the layered transition-metal dichalcogenides (MX_2: M = Mo or W, X = S or Se), WS_2 has graphite-like structure, consisting of two dimensional S-W-S layers that are hexagonally stacked by weak van der Waals interactions.[1,8] Electrons prefer to move along the basal plane of the S-W-S layers towards the edge sites that are favorable for the catalytic HER. The WS_2 catalyst showed reasonably good electrocatalytic activity with an overpotential of 140-260 mV at a current density of 10 mA cm^{-2}) (η_{10}) , but suffered from somewhat limited durability.[3,6,8,13,16] More excitingly, Levy and Boudart discovered "Pt-like" catalytic performance of the tungsten carbide phases, which is an alternative path for development of new noble-metal-free catalysts.[25] The tungsten carbides performing similarly to Pt in catalytic behavior resulted from the establishment of a "Pt-like" *d*-band electronic density of states by intercalation of carbon atoms into the tungsten lattice.[26] Consequently, the tungsten carbides demonstrated effective surface catalysis in many research domains, for example, cellulose conversion, methanol oxidation, water reduction, etc.[24,35,36] In addition, high tolerance to CO, N and S poisoning is another meritorious property of the tungsten carbides for replacement of precious metals in renewable energy systems, such as fuel cells and electrolyzers.[20,27,28]

It is therefore of considerable interest to fabricate low-cost and highly efficient tungsten-based catalysts for hydrogen fuel production. Although the tungsten carbides showed high HER performance, the solitary tungsten carbides exhibited limited durability in long-term catalytic reactions unless coupled with WN as a stabilizer.[4] In our previous research, we discovered highly efficient HER composite catalysts consisting of Mo_2C and Mo_2N by sintering soybean powder and ammonium molybdate.[29] The soybean provided C and N for forming both Mo_2C and Mo_2N in the catalysts, in which the Mo_2N imparted a strong stabilizing effect against corrosion in acids.

Thus, the long term durability of the HER by the MoSoy catalysts was significantly enhanced. Inspired by our previous work on biomass-derived MoSoy catalysts,[29] herein we report the synthesis of WSoy catalysts comprising tungsten carbides (WC and W_2C) and tungsten nitride (WN) decorated onto graphene for the HER by sintering abundant and environmentally friendly precursors, ammonium tungstate (AMT), soybean powder and graphene nanoplatelets (GnP). In the composite product, tungsten carbides and WN worked as catalysts and catalysis stabilizer, respectively, in the HER. Graphene acted as a good catalyst support because of two advantageous properties: first, graphene is able to impede particle growth of the catalyst, which is beneficial to obtain more reaction sites on the catalyst surface;[30,31] and second, owning to the high electron mobility (>15000 cm^2 V^{-1} S^{-1}) and graphene's inherent flexibility, it is a good medium for establishing contact and improving conduction between catalyst particles and electrodes.[31,32] With optimization of the contents of the graphene and soybean powder in the precursors, the composite product, $WSoy_{0.7}GnP_{1.0}$ was found to be the most highly active HER catalyst in both catalytic activity and stability among all $WSoy_xGnP_y$ electrocatalysts examined. This paper thereby introduces an easy and inexpensive method to synthesize high-performance biomass-derived HER catalysts.

2. Results and discussion

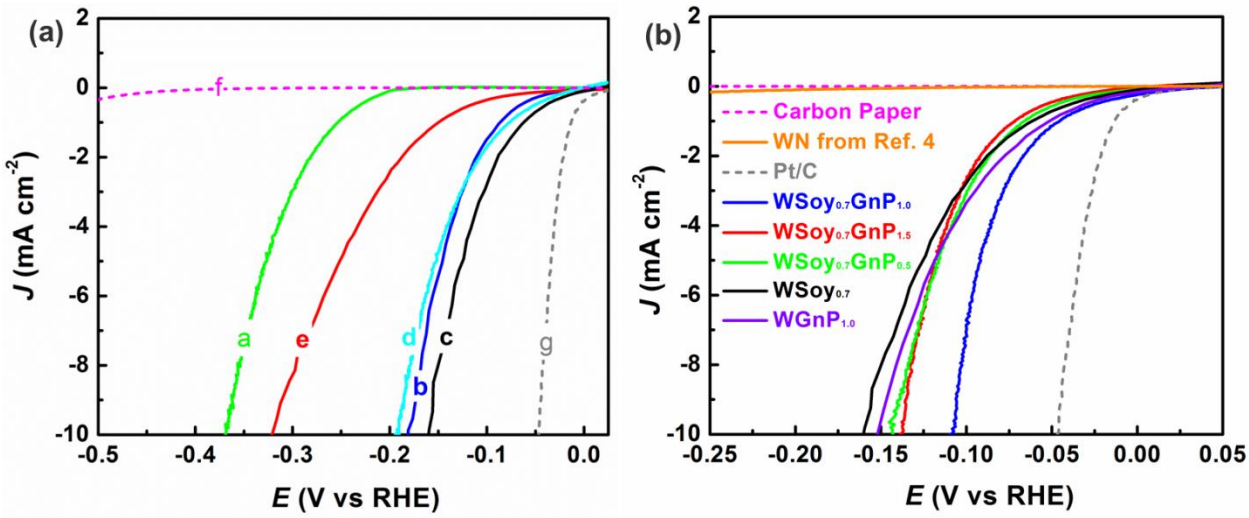

Figure 1. (a) Polarization curves of $WSoy_{0.2}$ (a), $WSoy_{0.5}$ (b), $WSoy_{0.7}$ (c), $WSoy_{1.0}$ (d), and $WSoy_{2.0}$ (e) samples, along with carbon paper without catalyst (f) and commercial Pt/C (g). **(b)** Polarization curves of $WSoy_{0.7}$,

$WSoy_{0.7}GnP_{0.5}$, $WSoy_{0.7}GnP_{1.0}$, $WSoy_{0.7}GnP_{1.5}$, and $WGnP_{1.0}$ samples, along with carbon paper without catalyst and commercial Pt/C. Also shown is the polarization curve of WN with a loading of 2.2 mg cm^{-2} from our previous research reported in reference 4. All the polarization curves were obtained in a H_2-purged 0.1 M $HClO_4$ aqueous solution with a scan rate of 2 mV s^{-1}. 10 mg of the samples were loaded onto each carbon paper electrode (1 cm^2). The loadings of W_2C, WC, and WN for $WSoy_{0.7}GnP_{1.0}$ $WSoy_{0.7}$, and $WGnP_{1.0}$ are listed in Table 1. The Pt loading on each electrode was 2 mg cm^{-2}.

Our methodology began with synthesis of a series of $WSoy_x$ (x=0.2, 0.5, 0.7, 1.0 and 2.0) to optimize the mass ratio of AMT and soybean powder. The detailed synthesis method is described in the Experimental section of the Supporting Information (SI). The electrochemical behavior for the HER of a series of the $WSoy_x$ catalysts is shown in Figure 1(a). The overpotential (η_{10}) was used to evaluate the HER activity of the electrocatalysts.[4,8,9] Among the five samples, the $WSoy_{0.7}$ showed the best HER performance with the smallest η_{10} of 0.16 V. Then, based on the $WSoy_{0.7}$ composition, three other catalysts ($WSoy_{0.7}GnP_{0.5}$, $WSoy_{0.7}GnP_{1.0}$ and $WSoy_{0.7}GnP_{1.5}$) with different graphene content were fabricated using the same method as described in the SI. As shown in Figure 1(b), all the $WSoy_{0.7}GnP_y$ samples had a smaller η_{10} than either $WSoy_{0.7}$ or $WGnP_{1.0}$ in the polarizationcurves. This indicates that both soybean and graphene can improve the electrocatalytic HER performance of the catalysts. Among the three catalysts of the $WSoy_{0.7}GnP_{0.5}$, $WSoy_{0.7}GnP_{1.0}$ and $WSoy_{0.7}GnP_{1.5}$ series, the $WSoy_{0.7}GnP_{1.0}$ showed significantly superior HER activity with a much smaller η_{10} of 0.105 V than the other two catalysts. We note that the bare carbon paper without catalyst did not show any HER activity as shown in both Figure 1(a) and 1(b).

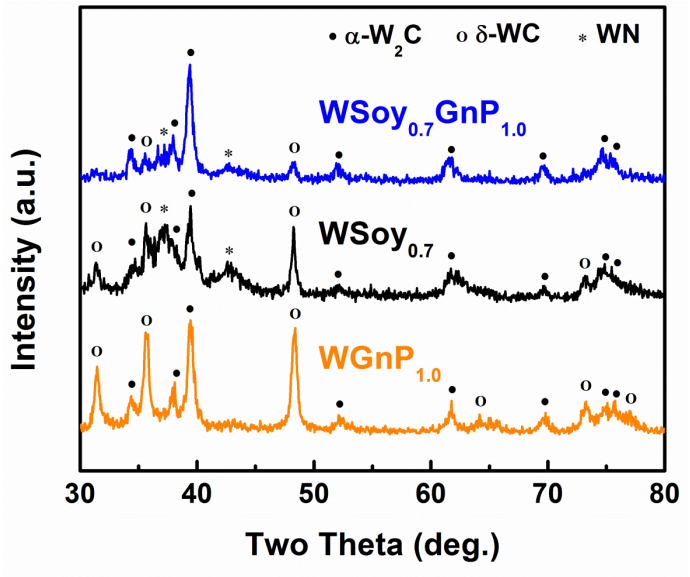

Figure 2. XRD patterns of the $WSoy_{0.7}GnP_{1.0}$, $WSoy_{0.7}$ and $WGnP_{1.0}$ samples. The assignments of the diffraction peaks are included (solid circle: α-W_2C, hollow circle: δ-WC, asterisk, WN).

To understand the effect of phase compositions of the catalysts on the HER, X-ray Diffraction (XRD) was employed to analyze three catalysts (Figure 2). The $WGnP_{1.0}$ catalysts consist of two tungsten carbides, α-W_2C (JCPDS: 35-0776) and δ-WC (JCPDS: 72-0097) without tungsten nitride because no soybean powder was present in the precursor mixture for supplying nitrogen. Both the $WSoy_{0.7}GnP_{1.0}$ and the $WSoy_{0.7}$ contain three tungsten compounds, α-W_2C, δ-WC, and WN (JCPDS: 65-2898). Phase fractions of the catalysts were obtained through Rietveld refinement (see SI for detailed information) of the XRD spectra, as shown in Figure S1 and Table S1. To obtain the mass content of each compound in the catalysts, the samples were analyzed with thermogravimetric analysis (TGA) by heating up to 950 ºC with a temperature ramping rate of 20 ºC min^{-1} in oxygen, and then the temperature was kept at 950 ºC for an extra 10 min to ensure the product was completely tungsten oxide (WO_3). The eventual WO_3 content of the $WSoy_{0.7}GnP_{1.0}$, $WSoy_{0.7}$ and $WGnP_{1.0}$ was 23%, 58%, and 72%, respectively, by weight normalization in Figure S2. With a total 10 mg sample loaded onto the carbon paper electrode, the masses of each compound are able to be calculated by using both WO_3 content and phase fractions,[4] which are shown in Table 1.

Table 1. Mass contents of the phases in the $WSoy_{0.7}GnP_{1.0}$, $WSoy_{0.7}$ and $WGnP_{1.0}$ samples on each electrode.

Sample	$WSoy_{0.7}GnP_{1.0}$ (mg cm^{-2})	$WSoy_{0.7}$ (mg cm^{-2})	$WGnP_{1.0}$ (mg cm^{-2})
W_2C	1.41	2.64	2.22
WC	0.34	2.76	2.61
WN	0.15	0.60	--
GnP + carbonizations	8.10	4.00	5.17

The mass of the tungsten carbides in the $WSoy_{0.7}GnP_{1.0}$ (W_2C, 1.41 mg; WC, 0.34 mg) was much smaller than that in the $WSoy_{0.7}$ (W_2C, 2.64 mg; WC, 2.76 mg) and $WGnP_{1.0}$ (W_2C, 2.22 mg; WC, 2.61 mg). This was due to a smaller amount of AMT in the precursor mixture of the $WSoy_{0.7}GnP_{1.0}$, which was also observed in the Mo_1Soy/RGO samples.[29] For example, the 33% ammonium molybdate in the precursor of Mo_1Soy/RGO led to 0.47 mg Mo_2C, however, 50% ammonium molybdate led to 1.40 mg Mo_2C in Mo_1Soy.[29] Our previous study[4] and a later study by Esposito et al.[23] showed that W_2C exhibited slight higher catalytic activity for the HER and a smaller Tafel slope than WC. However, WN more likely functioned as a stabilizer in the composite catalyst with considerably less catalytic HER activity than either the W_2C or the WC.[4] Comparing the $WSoy_{0.7}GnP_{1.0}$ and $WSoy_{0.7}$ compositions in Table 1, both catalysts contained W_2C, WC and WN. The tungsten carbides were even more abundant in the $WSoy_{0.7}$ than in the $WSoy_{0.7}GnP_{1.0}$, however, the η_{10} of the $WSoy_{0.7}$ (0.160 V) was larger than that of the $WSoy_{0.7}GnP_{1.0}$ (0.105 V). Actually, the graphene played an important role in the $WSoy_{0.7}GnP_{1.0}$ to function as a metal-like connector and carrier to establish more efficient charge transfer between the catalyst particles and the electrode.[30–32] Therefore, the reason that the $WSoy_{0.7}GnP_{1.0}$ performed better in the HER than the $WSoy_{0.7}$ even with less tungsten carbide content, is considered to stem from the interaction of the graphene-catalyst interface. These details are discussed below.

On the other hand, the $WSoy_{0.7}GnP_{1.0}$ catalyst, despite containing a very small amount of WN, showed a higher HER activity (η_{10} of 0.151 V) than that of the $WGnP_{1.0}$ (Figure 1), although the tungsten carbide content in $WSoy_{0.7}GnP_{1.0}$ was lower than that in $WGnP_{1.0}$ (Table 1). We note that $WGnP_{1.0}$ contains no WN phase. In our previous research, solitary WN

exhibited only a slight activity towards the HER, as shown in Figure 1(b).[4] Thus, the result of the present study suggests that in addition to acting as a stabilizer, WN may impart a synergistic effect to enhance the HER activity of the tungsten carbides even though the WN content involved is fairly small. There would be an electronic coupling between the nitride and carbides, although the detailed mechanism has yet to be explained but is being pursued.

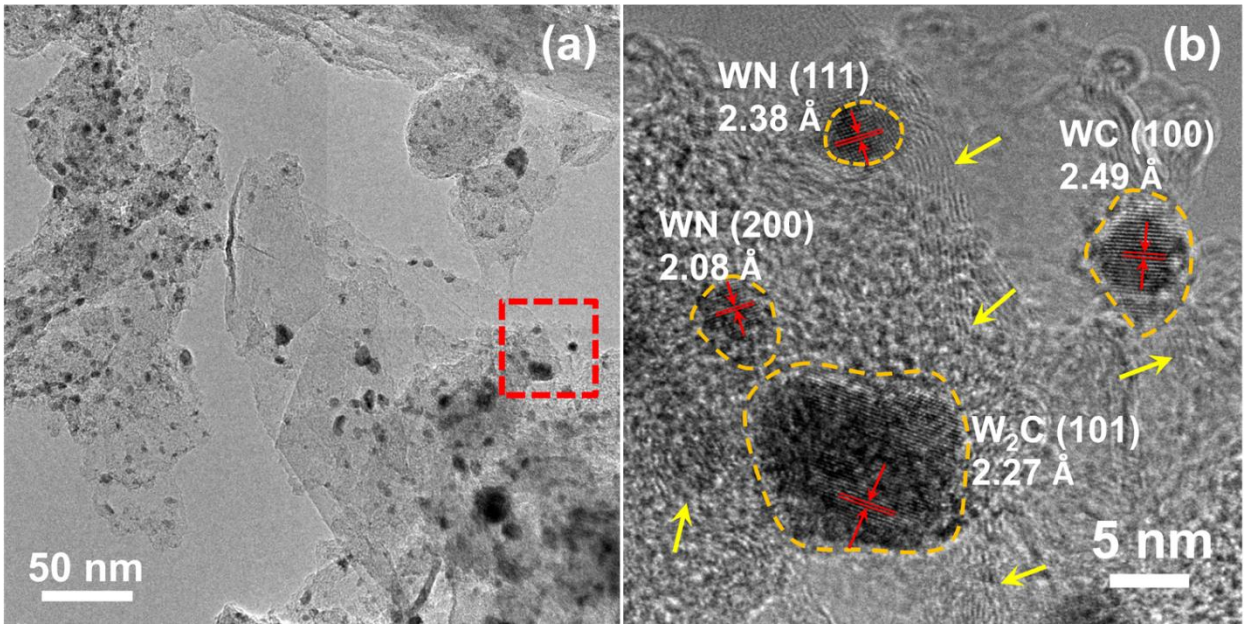

Figure 3. (a) TEM image of the $WSoy_{0.7}GnP_{1.0}$, and (b) HRTEM image of the enlarged area in the red box in (a)

The morphology of the $WSoy_{0.7}GnP_{1.0}$ is shown in the transmission electron microscope (TEM) images in Figure 3, which demonstrate the configuration and distribution of the various components. In Figure 3(a), the graphene nanoplatelets exhibit a size of 100–200 nm decorated by many black spots with a size between 5 and 20 nm. In order to clearly show the composition of the black spots, a high resolution transmission electron microscope (HRTEM) image is shown in Figure 3(b). Four nanoparticles are shown on the graphene nanoplatelets and are indicated by the dashed orange lines. The yellow arrows indicate the edges of the flexible layered structure of the nanoplatelets, while the red arrows identify the crystal facets on the surface of the nanoparticles. The largest nanoparticle is W_2C with a lattice spacing of 2.27 Å, which is the (101) facet according to the standard JCPDS: 35-0776. In addition, the WC shows a clear orientation of (100) with a spacing of 2.49 Å (JCPDS: 72-0097), and the other two small WN

particles exhibit crystal facets of (111) and (200) with spacings of 2.38 Å and 2.08 Å (JCPDS: 65-2898), respectively. The TEM and HRTEM images of the $WGnP_{1.0}$, and $WSoy_{0.7}$ catalysts are presented in Figure S3, in which the $WGnP_{1.0}$ shows similar morphology to that of the $WSoy_{0.7}GnP_{1.0}$ with decoration by W_2C and WC on the graphene nanoplatelets. The size of the tungsten carbides in the $WGnP_{1.0}$ sample is about 15 nm in Figures S3(b) and S3(c). However, most of the particles of the $WSoy_{0.7}$ catalyst grew up to ~ 20-50 nm as shown in Figure S3(d). The much larger particle size of the $WSoy_{0.7}$ than of the $WSoy_{0.7}GnP_{1.0}$ and the $WGnP_{1.0}$ is attributed to the absence of graphene nanoplatelets.[30,31] Thus, by comparison of the morphologies of the $WSoy_{0.7}$ and $WSoy_{0.7}GnP_{1.0}$, two merits of the graphene for enhancement of the electrocatalytic performance were demonstrated. First, graphene hindered particle growth of the tungsten carbides and nitrides, leading to more reaction sites on the catalyst surface for the HER. Second, graphene functioned as a good medium for charge transfer between the catalyst and electrodes. Given that the catalyst particles were grown on the graphene, and the catalysts were not directly attached onto the electrode, the electrons were still able to move from the electrode to the catalyst particles owing to the excellent conductivity and charge mobility in graphene. Without graphene, some electron transfer pathways are hindered by the interfaces of the particles because the interfaces can act as recombination sites for the charges.[2,32] Therefore, fewer electrons are used by the catalyst for the HER in the $WSoy_{0.7}$ than that in the $WSoy_{0.7}GnP_{1.0}$.

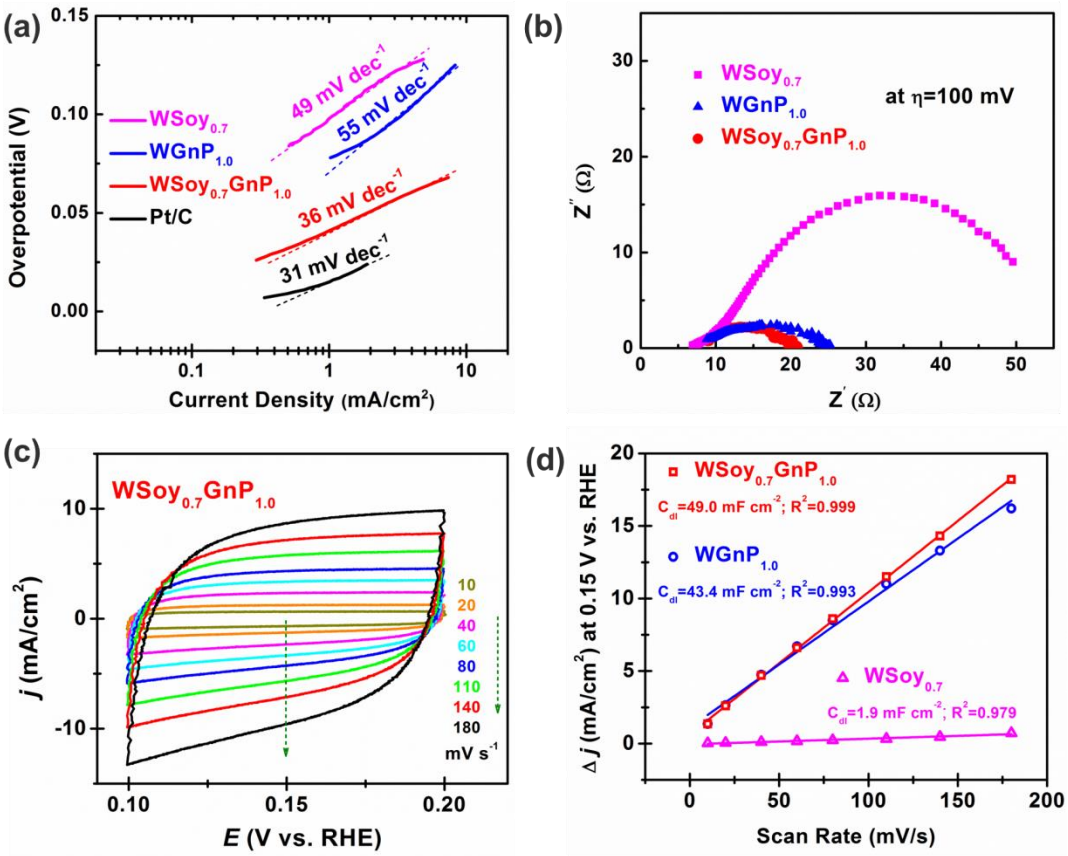

Figure 4. Electrochemical measurements on the catalysts: (a) Tafel plots; (b) electrochemical impedance spectroscopy (EIS) at a bias of 100 mV of $WSoy_{0.7}GnP_{1.0}$, $WSoy_{0.7}$ and $WGnP_{1.0}$; (c) cyclic voltammetry curves of $WSoy_{0.7}GnP_{1.0}$ in the region of 0.1-0.2 V; and (d) linear fitting of the capacitive currents of $WSoy_{0.7}GnP_{1.0}$, $WSoy_{0.7}$ and $WGnP_{1.0}$ vs. scan rate to obtain C_{dl} of each catalyst.

Table 2. Tafel slope and exchange current density calculated from the Tafel plots of the catalysts

Catalyst	Tafel Slope (mV dec^{-1})	Exchange Current Density (mA cm^{-2})
$WSoy_{0.7}GnP_{1.0}$	36	0.063
$WSoy_{0.7}$	49	0.011
$WGnP_{1.0}$	55	0.040
Pt/C	31	0.344

Electrochemical performance of the catalysts was evaluated as shown in the Figure 4. Tafel plots in Figure 4(a) were employed to calculate two indicators (Tafel slope and exchange current density) for characterizing the electrochemical HER process of the catalysts as shown in Table 2. In acidic aqueous media, the HER process is described in two steps according to different models of the two-electron reaction.[6,8,9] First, the Volmer reaction (also called the "discharge step") in which the combination of electrons and adsorbed protons on the active sites of the catalyst takes place, resulting in surface-bound hydrogen atoms. Then, the hydrogen molecules are released by electrochemical desorption (Heyrovsky reaction), or by recombination of hydrogen atoms absorbed on the catalysts surface (Tafel reaction).[6,9] The slope of the Tafel plot of the Pt/C catalyst was 31 mV dec^{-1}, which typifies the recombination of adsorbed hydrogen as the rate-limiting step.[21] However, the $WSoy_{0.7}$ and $WGnP_{1.0}$ catalysts had larger Tafel slopes of 49 and 55 mV dec^{-1}, respectively, suggesting a Volmer-Heyrovsky reaction with hydrogen electrochemical desorption as the rate-limiting step.[3,9] The $WSoy_{0.7}GnP_{1.0}$ gave rise to a Tafel slope of 36 mV dec^{-1} over a small overpotential range, suggesting a possible pathway of the Volmer-Tafel reaction.[3,9] Our $WSoy_{0.7}GnP_{1.0}$ sample has the smallest Tafel slope of any other tungsten-based catalysts reported to date in previous research, as shown in Table S2,[4,8,13,16,19,20,24] revealing that the $WSoy_{0.7}GnP_{1.0}$ showed faster proton discharge kinetics than the other counterparts.[5,29] Moreover, in Table 1, the exchange current density of the $WSoy_{0.7}GnP_{1.0}$ is determined to be 0.063 mA cm^{-2} by linear fitting of the Tafel plot, which was larger than the other two catalysts. The significantly reduced Tafel slope and increased exchange current density of the $WSoy_{0.7}GnP_{1.0}$ reflects a lower energy barrier and more accessibility of the electrocatalytic HER, which is consistent with the decreased overpotential and increased current density in the polarization curve in Figure 1. In addition, electrochemical impedance spectroscopy (EIS) was employed to investigate the charge transfer resistance (R_{ct}) of the HER on the electrodes at a bias of 100 mV. In Figure 4(b), the Nyquist plots indicate the R_{ct} of the $WSoy_{0.7}GnP_{1.0}$, $WSoy_{0.7}$ and $WGnP_{1.0}$.[4,8] The smaller R_{ct} of the $WSoy_{0.7}GnP_{1.0}$ and the $WGnP_{1.0}$ of 10.7 and 15 Ω, respectively, than that of the $WSoy_{0.7}$ of ~50 Ω indicates facile charge transfer towards the HER. Compared with other tungsten-based catalysts in Table S2, the $WSoy_{0.7}GnP_{1.0}$ ranked as one of the top-performing electrocatalysts. The $WSoy_{0.7}GnP_{1.0}$ showed smallest η_{10} and Tafel slope among all the W-based catalysts, suggesting the lowest energy barrier and fastest proton discharging, which can also be supported by its smaller R_{ct} than most of the others. Its rate-

limiting step is probably recombination (Tafel reaction) rather than electrochemical desorption (Heyrovsky reaction), reflecting "metal-like" behavior, which is consistent with the previous results of Pt-like surface catalysis performance.[25]

We also used the cyclic voltammetry (CV) method to evaluate the electrochemically active surface area of the catalysts, which demonstrated a proportional relationship with the double layer capacitance (C_{dl}) of the solid-liquid interface.[8,16,33,34] In Figures 4(c) and S4, the potential range between 0.10 V and 0.20 V was selected to measure the accurate C_{dl} on the CV curves with exclusion of faradaic current. The CV was carried out at various scan rates (10, 20, 40, 60, 80, 110, 140, and 180 mV s^{-1}). The difference between the positive and negative current density at the center of the potential range was obtained as a function of the scan rates as shown in Figure 4(d). The C_{dl} value of the catalysts was found to be equivalent to the slope of the plot of the half current density difference (Δj at 0.15 V vs. RHE in Figure 4(c)) over the scan rates. The $WSoy_{0.7}GnP_{1.0}$ and $WGnP_{1.0}$ exhibited C_{dl} values of 49.0 and 43.4 mF cm^{-2}, respectively, which was much larger than that of the WSoy (1.9 mF cm^{-2}). The increase in the C_{dl} value by a factor of *ca*. 25 arising from coupling graphene nanoplatelets with tungsten-based catalysts indicates a proliferation of catalytic sites of the catalyst/graphene composites. Since a very small C_{dl} value was obtained on graphene nanoplatelets only (1.1 mF cm^{-2}) in Figure S5, the high double layer capacitances of the $WSoy_{0.7}GnP_{1.0}$ and $WGnP_{1.0}$ are mostly attributed to an increase in surface area of the catalysts. Herein, the graphene plays a crucial role in hindering catalyst crystal growth, which serves as direct evidence of the much better electrocatalytic HER performance of the $WSoy_{0.7}GnP_{1.0}$ than that of the $WSoy_{0.7}$ in Figure 1. Although the $WSoy_{0.7}GnP_{1.0}$ and $WGnP_{1.0}$ had similar electrochemically active surface areas, the $WGnP_{1.0}$ showed less electrocatalytic activity for the HER. This is attributable to the absence of WN in the catalyst as we discussed above. Overall, as a catalyst carrier and conductive medium, the graphene can significantly boost the HER performance of the tungsten carbides by decreasing energy barrier, enhancing charge transfer and increasing the electrochemically active surface area of the catalyst.

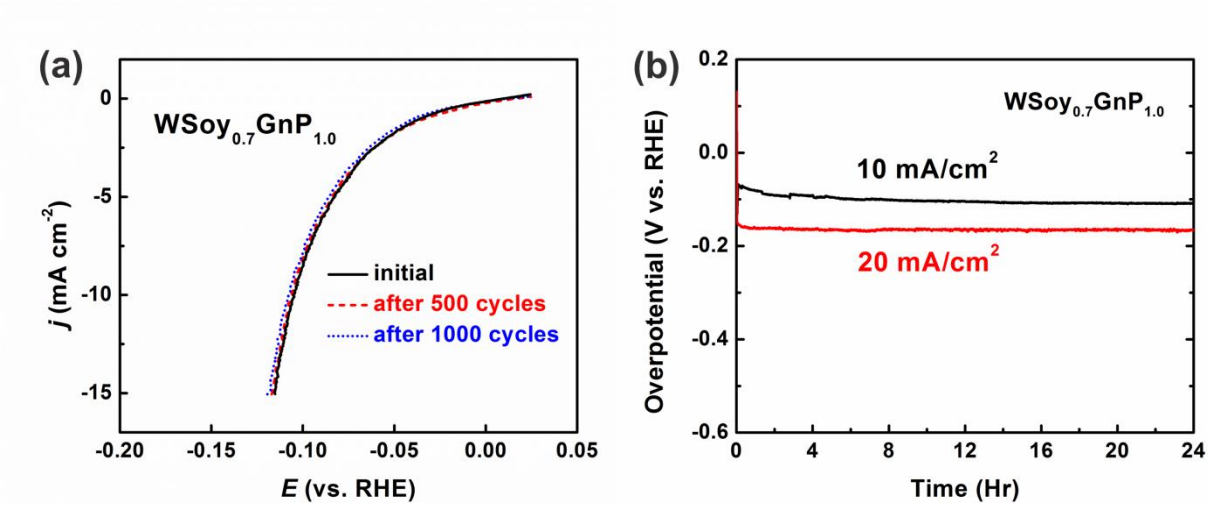

Figure 5. (a) Polarization curves of the $WSoy_{0.7}GnP_{1.0}$ before and after 500 and 1000 cycles at potentials between -0.5 V and +0.3 V with a scan rate of 200 mV s^{-1}; and (b) plots of overpotential vs. time for the $WSoy_{0.7}GnP_{1.0}$ electrode held for 24 hrs at a constant current density of 10 and 20 mA cm^{-2} (after *iR* correction). Both electrochemical experiments were conducted in a H_2-bubbled 0.1 M $HClO_4$ aqueous solution.

Figures 5(a) and S6 show the stability performance of the $WSoy_{0.7}GnP_{1.0}$, $WSoy_{0.7}$ and $WGnP_{1.0}$, which was investigated by potential cycle tests at potentials between -0.5 V and +0.3 V. In Figure 5(a), the three polarization curves of $WSoy_{0.7}GnP_{1.0}$ at initial, 500 and 1000 cycles are almost identical at potentials above -0.05 V; below -0.05 V, the curves are only slightly separated. However, in Figure S6, the $WSoy_{0.7}$ and $WGnP_{1.0}$ catalysts show increased overpotentials after 500 and 1000 cycles of the deterioration test. Without graphene, the stability performance of the $WSoy_{0.7}$ was slightly worse than that of the $WSoy_{0.7}GnP_{1.0}$. On the other hand, without soybean in the precursor mixture, the $WGnP_{1.0}$ deteriorated significantly after 500 and 1000 potential cycles. Therefore, the $WSoy_{0.7}GnP_{1.0}$ displays better electrochemical stability performance than either the $WSoy_{0.7}$ or the $WGnP_{1.0}$. In addition, chronopotentiometric measurements of the $WSoy_{0.7}GnP_{1.0}$ at a current density of 10 and 20 mA cm^{-2} are shown in Figure 5(b). The overpotentials at both constant current densities were fairly constant during electrolysis for 24 hours. As demonstrated in our previous research,[4] the stable electrochemical performance of the $WSoy_{0.7}GnP_{1.0}$ is also considered to result from the presence of the stabilizer WN in the catalyst.

In conclusion, we have developed a low-cost and high-performance tungsten-based catalyst by sintering AMT, soybean powder and graphene nanoplatelets at 850 ºC. After mass

ratio optimization, the $WSoy_{0.7}GnP_{1.0}$ demonstrated the best electrochemical HER performance with the smallest overpotential (η_{10} = 0.105 V) among all the $WSoy_xGnP_y$ catalysts examined. Also, the Tafel slope of the $WSoy_{0.7}GnP_{1.0}$ (36 mV dec^{-1}) indicates a possible Volmer-Tafel reaction pathway. The low charge transfer resistance (9 Ω) and high double-layer capacitance (49.0 mF cm^{-2}) of the $WSoy_{0.7}GnP_{1.0}$ suggest that graphene improves charge transfer kinetics and increases the number of catalytic reaction sites. In addition, the $WSoy_{0.7}GnP_{1.0}$ exhibited excellent stability in the electrochemical HER after a 1000 potential cycle test as well as the significant long-term durability of chronopotentiometric water splitting up to 24 hours. Owing to its excellent kinetics and stability properties, the $WSoy_{0.7}GnP_{1.0}$ catalyst stands out as one of the few top-performance candidates among all the tungsten-based catalysts for the electrochemical HER.

Acknowledgement

The TEM/HRTEM studies were carried out at the Center for Functional Nanomaterials, Brookhaven National Laboratory (BNL). The work at BNL was carried out under contract DE-SC00112704 with the U.S. Department of Energy, Office of Science, Office of Basic Energy Sciences.

References

(1) A. B. Laursen, S. Kegnas, S. Dahl and I. Chorkendorff, *Energy Environ. Sci.*, 2012, **5**, 5577–5591.

(2) A. Kudo and Y. Miseki, *Chem. Soc. Rev.*, 2009, **38**, 253–278.

(3) L. Cheng, W. J. Huang, Q. F. Gong, C. H. Liu, Z. Liu, Y. G. Li and H. J. Dai, *Angew. Chem. Int. Ed.*, 2014, **53**, 7860–7863.

(4) W. F. Chen, M. S. Schneider, K. Sasaki, C.H. Wang, J. Schneider, S. Iyer, S. Iyer, Y. Zhu, J. T. Mucherman and E. Fujita, *ChemSusChem*, 2014, **7**, 2414–2418.

(5) W. F. Chen, C. H. Wang, K. Sasaki, N. Marinkovic, W. Xu, J. T. Mucherman, Y. Zhu and R. R. Adzic, *Energy Environ. Sci.*, 2013, **6**, 943–951.

(6) H. T. Wang, D. S. Kong, P. Johanes, J. J. Cha, G. Y. Zheng, K. Yan, N. Liu and Y. Cui, *Nano Lett.*, 2013, **13**, 3426−3433.

(7) Y. Zhou, Z. Xie, K. A. Brown, D. J. Park, X. Zhou, P. Chen, M. Hirtz, Q. Y. Lin, V. P. Dravid, G. C. Schatz, Z. Zheng and C. A. Mirkin, *Small*. 2015, **11**, 913−917.

(8) A. S. Daniel, R. Caroline, F. Meng, A. Forticaux, R. J. Hamers and S. Jin, *Energy Environ. Sci.*, 2014, **7**, 2608–2613.

(9) W. F. Chen, J. T. Muckerman and E. Fujita, *Chem. Commun.*, 2013, **49**, 8896–8909.

(10) T. F. Jaramillo, K. P. Jorgensen, J. Bonde, J. H. Nielsen, S. Horch and I. Chorkendorff, *Science*, 2007, **317**, 100−102.

(11) W. C. Sheng, M. Myint, J. G. Chen and Y. S. Yan, *Energy Environ. Sci.*, 2013, **6**, 1509−1512.

(12) J. Turner, G. Sverdrup, M. K. Mann, P. C. Maness, B. Kroposki, M. Ghirardi, R. J. Evans and D. Blake, *Int. J. Energy Res.*, 2008, **32**, 379–407.

(13) D. Voiry, H. Yamaguchi, J. Li, R. Silva, D. Alves, T. Fujita, M. Chen, T. Asefa, V. B. Shenoy, G. Eda and M. Chhowalla, *Nat. Mater.*, 2013, **12**, 850−855.

(14) J. Lin, Z. Peng, G. Wang, D. Zakhidov, E. Larios, M. Yacaman and J. M. Tour, *Adv. Energy Mater.*, 2014, **4**, 1301875.

(15) C. L. Choi, J. Feng, Y. Li, J. Wu, A. Zak, R. Tenne and H. J. Dai, *Nano Res.*, 2013, **6**, 921–928.

(16) K. Xu, F. M. Wang, Z. X. Wang, X. Y. Zhan, Q. S. Wang, Z. Z. Cheng, M. Safdar and J. He, *ACS Nano*, 2014, **8**, 8468–8476.

(17) J. M. Velazquez, F. H. Saadi, A. P. Pieterick, J. M. Spurgeon, M. P. Soriaga, B. S. Brunschwig and N. S. Lewis, *J. Electroanal. Chem.*, 2014, **716**, 45–48.

(18) Z. H. Pu, Q. Liu, A. M. Asiri and X. Sun, *ACS Appl. Mater. Interfaces*, 2014, **6**, 21874–21879.

(19) J. M. McEnaney, C. Crompton, J. F. Callejas, E. J. Popczun, C. G. Read, N. S. Lewis and R. E. Schaak, *Chem. Commun.*, 2014, **50**, 11026–11028.

(20) S. T. Hunt, T. Nimmanwudipong and Y. Roman-Leshkov, *Angew. Chem. Int. Ed.*, 2014, **53**, 5131–5136.

(21) D. V. Esposito and J. G. Chen, *Energy Environ. Sci.*, 2011, **4**, 3900–3912.

(22) T. G. Kelly and J. G. Chen, *Chem. Soc. Rev.*, 2012, **41**, 8021–8034.

(23) D. V. Esposito, S. T. Hunt, Y. C. Kimmel and J. G. Chen, *J. Am. Chem. Soc.*, 2012, **134**, 3025−3033.

(24) H. Fei, Y. Yang, X. Fan, G. Wang, G. Ruan and J. M. Tour, *J. Mater. Chem. A*, 2015, **3**, 5798–5804.

(25) R. B. Levy and M. Boudart, *Science*, 1973, **181**, 547–549.

(26) L. H. Bennett, J. R. Cuthill, A. J. McAlister, N. E. Erickson and R. E. Watson, *Science*, 1974, **184**, 563–565.

(27) D.R. McIntyre, G.T. Burstein and A. Vossen, *J. Power Sources*, 2002, **107**, 67–73.

(28) J. G. Chen, *Chem. Rev.*, 1996, **96**, 1477–1498.

(29) W. F. Chen, S. Iyer, S. Iyer, K. Sasaki, C. H. Wang, Y. Zhu, J. T. Muckerman and E. Fujita, *Energy Environ. Sci.*, 2013, **6**, 1818–1826.

(30) F. K. Meng, J. T. Li, S. K. Cushing, J. Bright, M. J. Zhi, J. D. Rowley, Z. L. Hong, A. Manivannan, A. D. Bristow and N. Q. Wu, *ACS Catal.*, 2013, **3**, 746–751.

(31) F. K. Meng, J. T. Li, S. K. Cushing, M. J. Zhi and N. Q. Wu, *J. Am. Chem. Soc.*, 2013, **135**, 10286−10289.

(32) I. V. Lightcap, T. H. Kosel and P. V. Kamat, *Nano Lett.*, 2010, **10**, 577–583.

(33) G. Q. Lu and J. T. Yates, *Chem. Rev.*, 1995, **95**, 735–758.

(34) C. L. McCrory, S. Jung, I. M. Ferrer, S. M. Chatman, J. C. Peters and T. F. Jaramillo, *J. Am. Chem. Soc.*, 2015, **137**, 4347−4357.

(35) R. Ganesan and J. S. Lee, *Angew. Chem. Int. Ed.*, 2005, **44**, 6557–6560.

(36) N. Ji, T. Zhang, M. Zheng, A. Wang, H. Wang, X. Wang and J. G. Chen, *Angew. Chem. Int. Ed.*, 2008, **47**, 8510–8513.

Supporting Information

Biomass-Derived High-Performance Tungsten-Based Electrocatalyst on Graphene for Hydrogen Evaluation

Fanke Meng,[a] Enyuan Hu,[a] Lihua Zhang,[b] Kotaro Sasaki,[a,]*

James T. Muckerman,[a] and Etsuko Fujita[a,]*

[a] Chemistry Department, Brookhaven National Laboratory, Upton, New York, 11973, USA.

[b] Center for Functional Nanomaterials, Brookhaven National Laboratory, Upton, New York 11973, USA

Experimental

1 Synthesis of tungsten-based composite catalysts

Graphene-supported tungsten-based composites ($WSoy_xGnP_y$, x and y are mass ratios of the soybean and graphene nanoplatelets) were prepared by sintering powdered mixtures of graphene nanoplatelets (GnP, xGnP® C-750 from XG Sciences) with ammonium tungstate (AMT, $(NH_4)_{10}H_2(W_2O_7)_6 \cdot 4H_2O$, Aldrich) and soybean (organic yellow dry soybeans supplied by the Whole Food Market, Inc.) powder.

The mass ratio of soybean over AMT was optimized firstly. The detailed procedure is described as follows. First, the soybean was ground to a powder and mixed with AMT. The mass ratios of soybean over AMT were 0.2, 0.5, 0.7, 1.0, and 2.0 respectively. For a typical example, 200 mg of AMT was mixed with 40 mg, 100 mg, 140 mg, 200 mg, and 400 mg of soybean respectively. Second, the mixtures were added into deionized (DI) water and ultrasonicated for 40 min to form uniform suspensions. Third, the suspensions were dried in an oven at 90 °C overnight. Fourth, the dried powders were sintered at 850 °C in argon for 2 hrs in a quartz tube furnace to obtain black catalyst powders for the following experiments. Among all the samples ($WSoy_{0.2}$, $WSoy_{0.5}$, $WSoy_{0.7}$, $WSoy_{1.0}$ and $WSoy_{2.0}$), the $WSoy_{0.7}$ exhibited the smallest overpotential (η_{10}). Consequently, the content of graphene was tuned in the order of $WSoy_{0.7}GnP_{0.5}$, $WSoy_{0.7}GnP_{1.0}$ and $WSoy_{0.7}GnP_{2.0}$. As a comparison, $WGnP_{1.0}$ was synthesized using the same method.

2 Electrochemical measurements

The electrochemical polarization curves of the catalyst samples were measured with VersaSTAT 3 Potentiostate (Princeton Applied Research) in a three-electrode configuration cell, in which the catalyst, platinum and Ag/AgCl/KCl (3 M) acted as working electrode, counter electrode and reference electrode, respectively. All potentials were quoted with respect to reversible hydrogen electrode (RHE), and all the polarization curves were *iR*-corrected according to ohmic resistance obtained in the electrochemical impedance spectroscopy (EIS) measurement. Typically, 10 mg of catalyst powder was mixed with 5 drops of 20 % Nafion dispersion (DuPont) to form homogenous slurry. The slurry was pasted onto 1 cm^2 carbon paper (Toray TGP-H-060. The size of the carbon paper was 1 cm × 3 cm, on which a 1 × 1 cm^2 area was exposed for slurry loading). After dried, the carbon paper loaded with catalyst was immersed into

0.1 M $HClO_4$ (aq.) electrolytes for electrochemical experiments. As a reference, the Pt/C was loaded onto a carbon paper electrode (diameter of 3 mm). The Pt/C (plot (g) in Figure 1(a)) was commercially available from BASF Inc. (20 % HP Pt on Vulcan XC-72R). The electrolyte solution was always bubbled with H_2 during the measurements.

The polarization curves for the hydrogen evolution reaction (HER) were obtained at a scan rate of 2 mV s^{-1}. The long-term stability tests were performed by potential cycling between -0.5 V and +0.3 V at a scan rate of 200 mV s^{-1}. The EIS measurements were conducted with a frequency from 100000 Hz to 0.01 Hz to determine ohm resistance (R_s) and charge-transfer resistance (R_{ct}). The double layer capacitances were tested using a glassy carbon electrode with a sample loading of 10 mg cm^{-2}.

3 Material Characterization

The morphology of the samples was obtained by transmission electron microscope (TEM, JEOL JEM 2100F). To prepare the TEM sample, 2 mg of catalyst was dissolved into 5 mL ethanol by ultrasonication for half minute to achieve a uniform suspension. Then, the suspension was dropped onto a carbon grid (Ted Pella, Inc.), which was thereafter dried in air for observation under TEM. The crystal structure and phase composition were obtained by a high-resolution TEM (HRTEM) and X-ray diffraction (XRD, Rigaku Ultima III) with Cu Kα radiation (λ = 1.542 Å). The three phases in the catalysts were assigned to be α-W_2C, δ-WC, and WN with the major XRD peaks at 39.6º (101) (JCPDS: 35-0776), 35.6º (100) (JCPDS: 72-0097), 37.7º (111) (JCPDS: 65-2898), respectively. Thermogravimetric Analysis (TGA, Perkin Elmer Diamond) was conducted by heating the samples in oxygen flow (100 sccm) up to 950 ºC from room temperature. Then, the samples were kept in oxygen at 950 ºC for 10 min to ensure that all the samples were changed to tungsten oxide. The contents of each phase in the catalysts were calculated by using Rietveld-refined XRD spectra and TGA results.[1] The method of Rietveld refinement is briefly introduced in the following experimental section 4.

4 Rietveld refinement of the XRD data

Rietveld refinement was carried out using the software GSAS-EXPGUI.[2,3] The refinement is based on the model that physically describes the peak position and peak intensity and semi-empirically describes the peak shape. The peak position is mainly determined by the

lattice constant and x-ray wavelength according to Bragg's law and the peak intensity is mainly determined by atomic positions, atomic vibrations and phase fraction. The peak shape is modeled using a pseudo-Voigt function which is a linear combination of Gaussian function and Lorentzian function. Physical parameters and parameters of describing the peak shape are refined to yield the most satisfactory description of the whole XRD pattern. Phase fraction information is thus obtained.

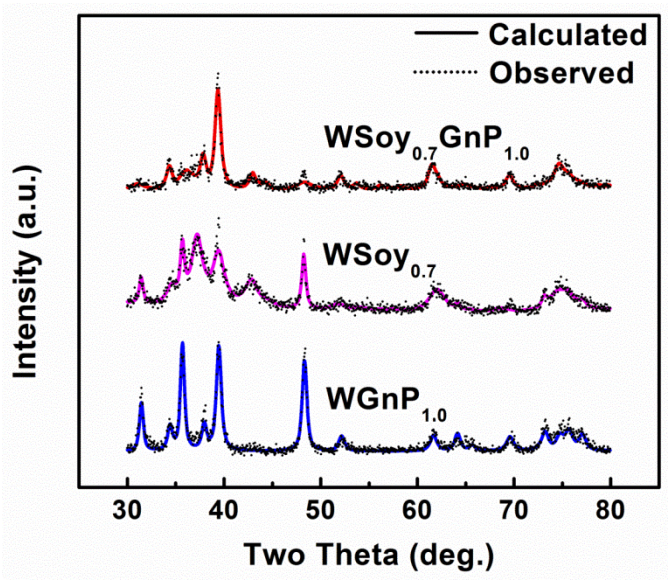

Figure S1. XRD spectra of the samples and Rietveld refined spectra

Table S1. Mass ratio of the W_2C, WC and WN phases in $WSoy_{0.7}GnP_{1.0}$, $WSoy_{0.7}$ and $WGnP_{1.0}$.

Sample	$WSoy_{0.7}GnP_{1.0}$	$WSoy_{0.7}$	$WGnP_{1.0}$
W_2C	0.74	0.44	0.46
WC	0.18	0.46	0.54
WN	0.08	0.1	--

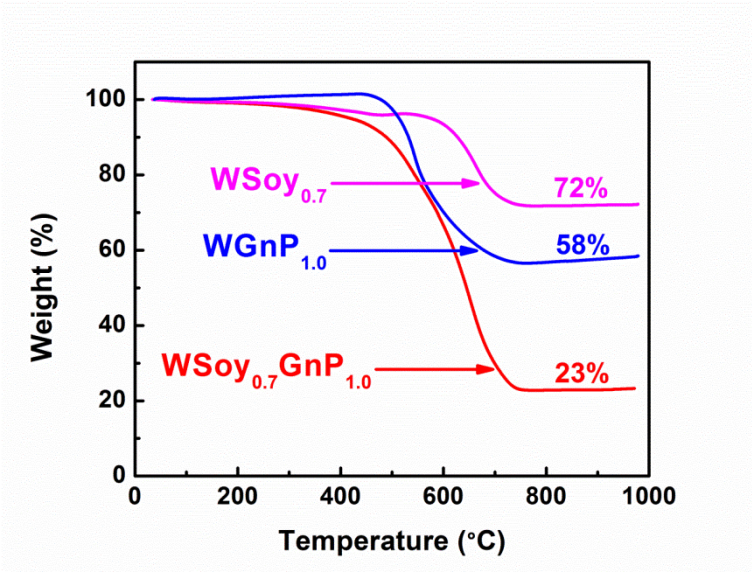

Figure S2. TGA thermogramms of the $WSoy_{0.7}GnP_{1.0}$, $WSoy_{0.7}$ and $WGnP_{1.0}$ samples.

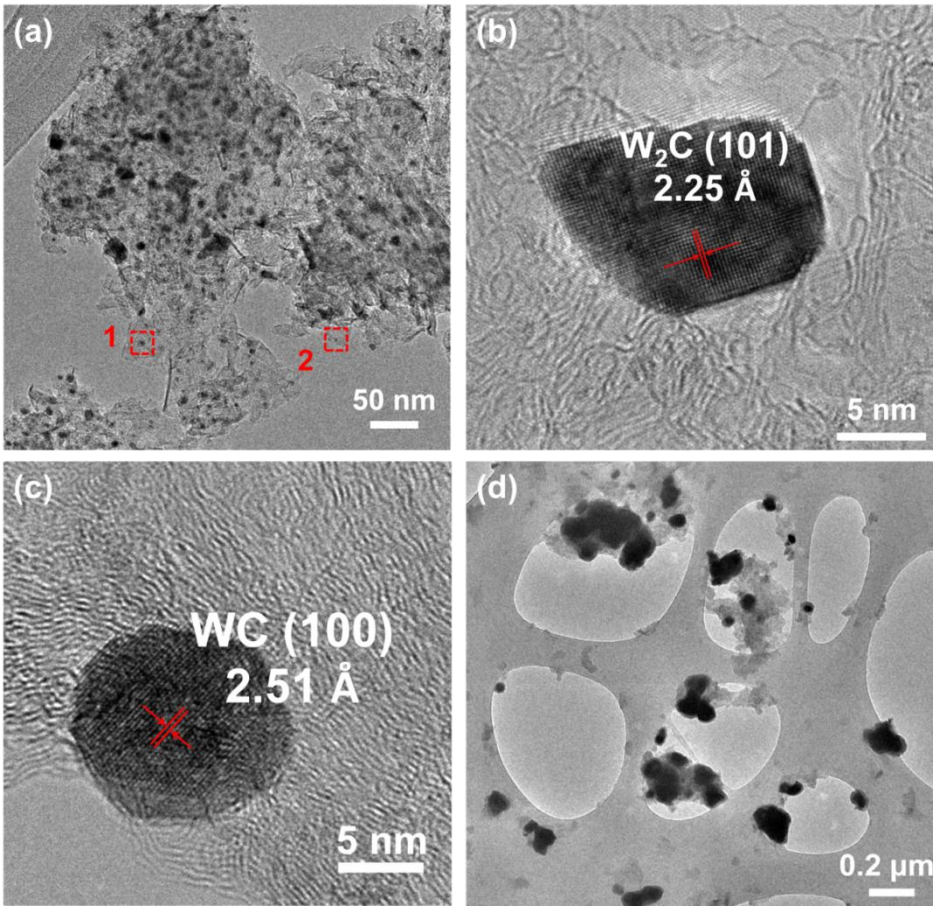

Figure S3. TEM and HRTEM images of the $WGnP_{1.0}$ (a)-(c), and $WSoy_{0.7}$ (d). The HRTEM images in (b) and (c) show the area of the red squares labeled 1 and 2, respectively, in image (a) indicating decoration of W_2C and WC nanoparticles on the graphene nanoplatelets.

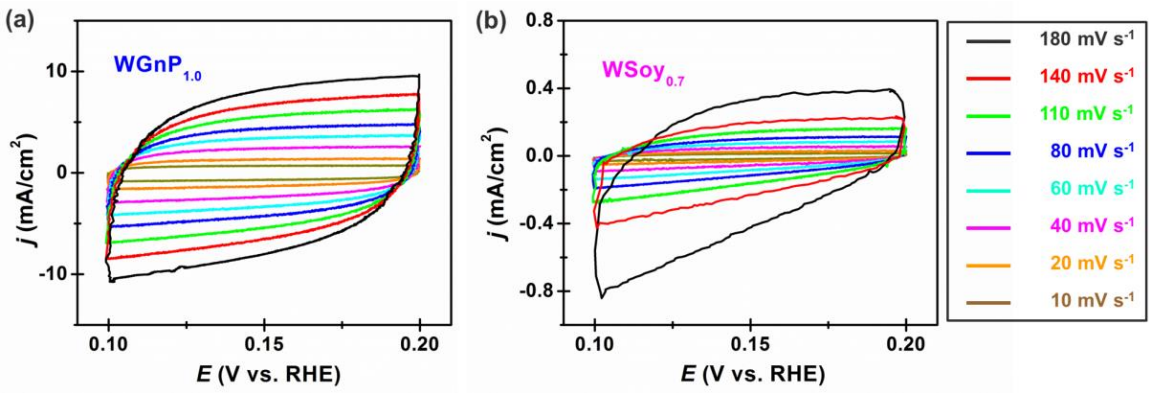

Figure S4. Cyclic voltammetry curves of the $WGnP_{1.0}$ and $WSoy_{0.7}$ in the region of 0.1-0.2 V.

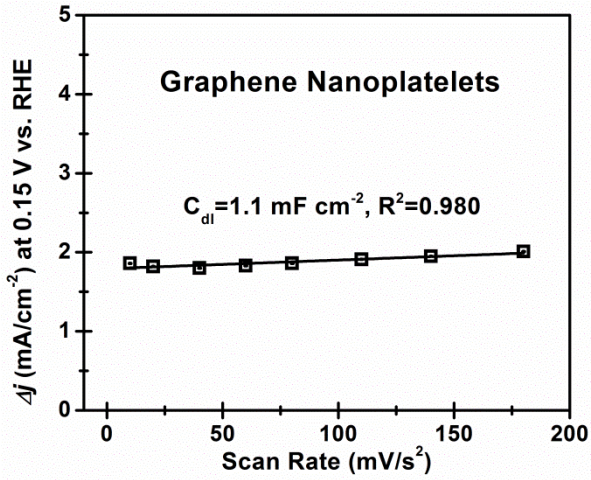

Figure S5. Liner fitting of the capacitive current of the graphene nanoplatelets vs. the scan rate to obtain the C_{dl}.

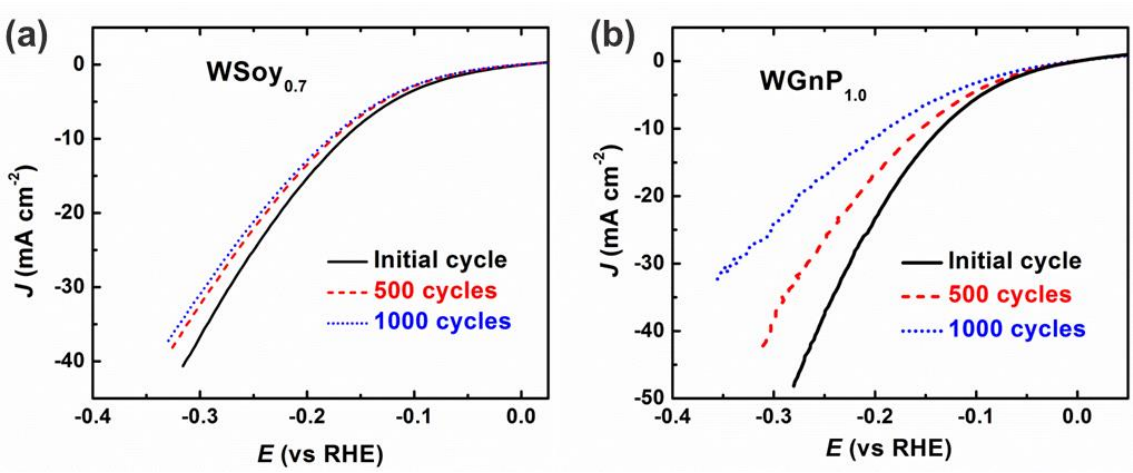

Figure S6. Polarization curves of the $WSoy_{0.7}$ and $WGnP_{1.0}$ catalysts before and after 500 and 1000 cycles at potentials between -0.5 V and +0.3 V with a scan rate of 200 mV s^{-1}.

Table S2. Comparison of different W-based HER electrocatatlysts available from literatures.

Catalyst	Overpotential (η_{10}), mV	Tafel slope, mV dec^{-1}	Exchange Current Density, 10^{-2} mA cm^{-2}	R_{ct}, Ω	Stability	Ref.
$WSoy_{0.7}GnP_{1.0}$	105	36	6.3	10.7 @ 100 mV	1000 cycles, 24 hrs Chronopotentialmetric electrolysis, stable	This study
α-WC/carbon black	260	N/A	N/A	N/A	3000 cycles,stable	4
W_2C microsphere	~ 170 (a)	118	28.1	N/A	N/A	5
Commercial WC	~ 300 (a)	73	1.8	N/A	N/A	5
$W_{0.5}$Ani/GnP	120	68.6 (b)	3.8	12.7@100 mV	10000 cycles, stable	1
W_2C/GnP	186	64.7 (b)	2.4	15.6@100 mV	5000 cycles, not stable	1
Bulk W_2C	336	88.0 (b)	0.065	1750@100 mV	N/A	1
WN	>500	N/A	N/A	N/A	5000 cycles, stable	1
Thin film W_2C	>300 (c)	69	0.02	N/A	N/A	6
Thin film WC	> 400 (c)	91	0.25	N/A	N/A	6
WS_2 nanosheets	~ 160	72	0.25	N/A	1000 cycles, stable	7
Exfoliated 1T WS_2	~260 (a)	~55	2.0	>250 @100 mV	>10000 cycles, stable	8
WS_2/rGO hybrid nanosheets	~260 (a)	58	<0.1 (d)	~200	N/A	9
metallic WS_2 nanosheets	142	70	N/A	5 @250 mV	500 cycles, slight loss in catalytic activity	10
WS_2 nanoflakes	~150 (a)	48	N/A	N/A	10000 cycle, slight loss in catalytic activity	11
WS_2 nanoribbons	225	68	1.25	38 @250 mV, >2000 @100 mV	1000 cycle, stable	12
WSe_2 on carbon fiber paper	300	77.4	N/A	N/A	15000 cycle, stable	13
WSe_2	~350 (a)	99	0.3	624 @128 mV	Potentiostatic electrolysis for 7000 s, stable	14

$W(S_{0.48}Se_{0.52})_2$	~260 (a)	105	2.9	204@128 mV	Potentiostatic electrolysis for 7000 s, stable	14
Amorphous WP	~120 (a)	54	4.5	N/A	500 cycles 18 hr, 100 mV/s stable	15
P-modified WN/rGO	85	54	35	N/A	5000 cycles, slight loss in catalytic activity	16
WC on vertically aligned CNTs	145	72	~10 (d)	N/A	1000 cycles, slight loss in catalytic activity	17

(a) The overpotential (η_{10}) was estimated from *JV* polarization curves.
(b) The Tafel slope was obtained from plots of E vs. $\log(R_{ct})^{-1}$.
(c) The overpotential (η_{10}) was estimated from Tafel plots.
(d) The exchange current density was estimated from Tafel plots.

References

(1) W. F. Chen, M. S. Schneider, K. Sasaki, C. H. Wang, J. Schneider, S. Iyer, S. Iyer, Y. Zhu, J. T. Mucherman and E. Fujita, *ChemSusChem*, 2014, **7**, 2414–2418.

(2) "Gsas." General Structure Analysis System, A.C. Larson, R.B. Von Dreele. LANSCE, MS-H805, Los Alamos, New Mexico (1994).

(3) EXPGUI, a graphical user interface for GSAS, B.H. Toby, J. Appl. Crystallogr., 2001, 34 , 210-213.

(4) S. T. Hunt, T. Nimmanwudipong and Y. Roman-Leshkov, *Angew. Chem. Int. Ed.*, 2014, **53**, 5131–5136.

(5) D. J. Ham, R. Ganesan and J. S. Lee, *Int. J. Hydrogen Energy*, 2008, **33**, 6865–6872.

(6) D. V. Esposito, S. T. Hunt, Y. C. Kimmel and J. G. Chen, *J. Am. Chem. Soc.*, 2012, **134**, 3025−3033.

(7) Z. Wu, B. Fang, A. Bonakdarpour, A. Sun, D. P. Wilkinson and D. Wang, *Appl. Catal., B.*, 2012, **125**, 59–66.

(8) D. Voiry, H. Yamaguchi, J. Li, R. Silva, D. Alves, T. Fujita, M. Chen, T. Asefa, V. B. Shenoy, G. Eda and M. Chhowalla, *Nat. Mater.*, 2013, *12*, 850–855.

(9) J. Yang, D. Voiry, S. J. Ahn, D. Kang, A. Kim, M. Chhowalla and H. Shin, *Angew. Chem. Int. Ed.*, 2013, **52**, 13751–13754.

(10) A. S. Daniel, C. R. English, F. Meng, A. Forticaux, R. J. Hamers and S. Jin, *Energy Environ. Sci.*, 2014, **7**, 2608–2613.

(11) L. Cheng, W. J. Huang, Q. F. Gong, C. H. Liu, Z. Liu, Y. G. Li and H. J. Dai, *Angew. Chem. Int. Ed.*, 2014, **53**, 7860–7863.

(12) J. Lin, Z. Peng, G. Wang, D. Zakhidov, E. Larios, M. Yacaman and J. M. Tour, *Adv. Energy Mater.*, 2014, **4**, 1301875.

(13) H. T. Wang, D. S. Kong, P. Johanes, J. J. Cha, G. Y. Zheng, K. Yan, N. Liu and Y. Cui, *Nano Lett.*, 2013, **13**, 3426−3433.

(14) K. Xu, F. M. Wang, Z. X. Wang, X. Y. Zhan, Q. S. Wang, Z. Z. Cheng, M. Safdar and J. He, *ACS Nano*, 2014, **8**, 8468−8476.

(15) J. M. McEnaney, C. Crompton, J. F. Callejas, E. J. Popczun, C. G. Read, N. S. Lewis and R. E. Schaak, *Chem. Commun.*, 2014, **50**, 11026–11028.

(16) H. Yan, C. Tian, L. Wang, A. Wu, M. Meng, L. Zhao, H. Fu, *Angew. Chem. Int. Ed.*, 2015, **54**, 6325–6329.

(17) X. Fan, H. Zhou, X. Guo, *ACS Nano*, 2015, **9**, 5125–5134.